photoexcited, and metal atom insertion into the CN bond of the adducted diazomethane occurs. Finally, it would be of interest to compare the force constants of the CuC stretch in $CuCH_2$ and $CuCH_3$; however, some uncertainty exists with respect to the assigned CuC stretching mode for $CuCH_3$.[8] When this value is available it will be possible to assess the degree of double-bond character in the Cu–C bond of $CuCH_2$.

Acknowledgment. The financial support of the National Science Foundation, the Robert A. Welch Foundation, and the 3M Company are greatly appreciated. We gratefully acknowledge the assistance of Tom A. Holme with the UHF calculations of $CuCH_2$.

Registry No. $CuCH_2$, 108295-75-6; $Cu^{13}CH_2$, 108295-76-7; CuCHD, 108295-77-8; $CuCD_2$, 108295-78-9; N_2CuCH_2, 108295-79-0; $N_2Cu^{13}CH_2$, 108295-80-3; N_2CuCHD, 108295-81-4; N_2CuCD_2, 108295-82-5; Cu, 7440-50-8; N_2CH_2, 334-88-3; Ar, 7440-37-1; N_2, 7727-37-9.

Solid-State ^{31}P NMR Studies of DNA Liquid Crystalline Phases. The Isotropic to Cholesteric Transition†

Teresa E. Strzelecka and Randolph L. Rill*

Contribution from the Department of Chemistry and Institute of Molecular Biophysics, Florida State University, Tallahassee, Florida 32306. *Received December 11, 1986*

Abstract: Aqueous solutions of short DNA fragments with Na^+ as counterion form a cholesteric liquid crystalline phase when the DNA concentration exceeds a critical value dependent on DNA length and solution ionic strength. Transitions of solutions of 146 base pair (ca. 500-Å) length DNA between cholesteric and isotropic phases were monitored by ^{31}P solid-state NMR spectroscopy and polarizing microscopy. Isotropic phase formation upon increase of temperature or decrease of DNA concentration was indicated by the appearance of a sharp isotropic resonance superimposed on a broad resonance of the anisotropic phase. A phase diagram for transitions between isotropic and cholesteric phases in buffered DNA solutions with a sodium ion activity of 0.21 M was calculated from integrated areas of the isotropic and cholesteric phase resonances. The phase diagram is in good agreement with that predicted by the lattice statistics treatment of phase equilibria in solutions of weakly interacting, nonelectrolyte, rodlike particles by Flory. The fully isotropic and cholesteric phase boundaries are only weakly dependent on temperature and are separated by a narrow biphasic region in which the two phases coexist. At 20 °C the solutions were biphasic at DNA concentrations from 125 to 155 mg/mL and fully liquid crystalline above 155 mg/mL. The observed DNA phase boundaries agreed well with Flory's theory of noninteracting rods assuming a best-fit effective DNA radius of 21.5 ± 1 Å, in good agreement with the effective DNA radius determined at approximately this ionic strength by other methods employing scaled particle theory. This agreement suggests that isotropic to liquid crystalline phase transitions of semirigid polyelectrolytes modeled as scaled particles can be treated to a good first approximation in terms of Flory's theory. Preliminary evidence for a higher order DNA phase is also presented.

DNA concentrations in vivo range from a few milligrams per milliliter in eukaryotic chromatin to over 70% in phage and sperm heads; hence understanding of mechanisms of DNA packing in vivo requires knowledge of the behavior of highly concentrated DNA solutions. As first described by Onsager[1] and elaborated by Flory and others,[2] rodlike and semirigid polymers are expected to form ordered, liquid crystalline-like phases above some critical volume fraction due to the dominance of excluded volume effects. This behavior has been well documented for synthetic, nonelectrolyte polymers,[3] but not for polyelectrolytes. DNA and other semirigid, polyelectrolyte biopolymers are expected to order analogously to uncharged polymers due to the same dominance of excluded volume effects. The necessity for counterion screening of the high charge density on DNA introduces a complicating factor, however, since the condensed counterion atmosphere will contribute to the effective particle radius and hence to the effective axial ratio and volume fraction.[4]

Recent studies have shown that short DNA fragments in vitro in aqueous solutions with K^+, Na^+, or Mg^{2+} as supporting counterion can exist in at least two different condensed or aggregated phases depending on DNA concentration, ionic strength, and temperature. A gel-like phase occurs in solutions of Na^+ DNA and Mg^{2+} DNA with concentrations up to 35 mg/mL.[5] More concentrated DNA solutions form phases with cholesteric-like liquid crystalline order.[4a,6] Cholesteric-like organization has also been observed in solutions of high molecular weight DNA and in chromosomes of lower organisms such as dinoflagellates.[7] Evaluation of mechanisms leading to spontaneous cholesteric ordering of DNA is therefore important for understanding DNA condensation in vivo and the more general behavior of solutions of semirigid polyelectrolytes.

We have used solid-state ^{31}P NMR methods to obtain the first quantitative phase diagram for the isotropic to cholesteric tran-

†This work was supported in part by grants from the Department of Energy (EV05888) and the National Institutes of Health (GM37098).

*To whom reprint requests should be addressed at the Department of Chemistry.

(1) Onsager, L. *Annu. Rev. Biochim.* **1949**, *51*, 627–659.
(2) (a) Flory, P. J. *Proc. R. Soc. London, Ser. A* **1956**, *234*, 60–73, 73–89. (b) Flory, P. J. In *Polymer Liquid Crystals*; Ciferri, A., Krigbaum, W. R., Meyer, R. B., Eds.; Academic: New York, 1982; pp 103–112 and references cited therein. (c) Lasher, G. *J. Chem. Phys.* **1970**, *53*, 4141–4146.
(3) (a) Robinson, C. *Trans. Faraday Soc.* **1956**, *52*, 571–592; also *Faraday Soc. Discuss.* **1958**, *25*, 29–41. (b) Miller, W. *Annu. Rev. Phys. Chem.* **1979**, *29*, 219 and references cited therein.
(4) (a) Brian, A. A.; Frisch, H. L.; Lerman, L. S. *Biopolymers* **1981**, *20*, 1305–1328. (b) Stigter, D. *Biopolymers* **1977**, *16*, 1435–1448; also *J. Phys. Chem.* **1978**, *82*, 1603–1606. (c) Record, T. M.; Anderson, C. F.; Lohman, T. M. *Q. Rev. Biophys.* **1978**, *11*, 1–3–178. (d) Le Bret, M.; Zimm, B. H. *Biopolymers* **1984**, *23*, 271–285, 286–312.
(5) Fried, M. G.; Bloomfield, V. A. *Biopolymers* **1984**, *23*, 2141–2155.
(6) (a) Rill, R. L.; Hilliard, P. R., Jr.; Levy, G. C. *J. Biol. Chem.* **1983**, *258*, 250–256. (b) Rill, R. L. *Proc. Natl. Acad. Sci. U.S.A.* **1986**, *83*, 342–346. (c) Brandes, R.; Kearns, D. R. *Biochemistry* **1986**, *25*, 5890–5895.
(7) (a) Robinson, C. *Tetrahedron* **1961**, *13*, 219. (b) Luzzati, V.; Nicolaieff, A.; Masson, F. *J. Mol. Biol.* **1961**, *3*, 185–201. (c) Maniatis, T.; Venable, J. H.; Lerman, L. S. *J. Mol. Biol.* **1974**, *84*, 37–64. (d) Iizuka, E. *Polym. J.* **1977**, *9*, 173–180; also *10*, 235–237, 293–300. (e) Iizuka, E.; Kondo, Y. *Mol. Cryst. Liq. Cryst.* **1979**, *51*, 285–294. (f) Livolant, F. *Eur. J. Cell Biol.* **1984**, *33*, 300–311.

0002-7863/87/1509-4513$01.50/0

sitions of defined length DNA fragments in solutions of well-defined sodium activity. The overall shape of the phase diagram is in good agreement with the observed and predicted behavior of rodlike nonelectrolytes with repulsive interactions. The effective volume fractions for phase separation are in good quantitative agreement with the prediction of the lattice statistics theory of Flory[2a] assuming a reasonable value for the effective DNA radius.

Experimental Section

DNA Isolation. Short DNA fragments with a narrow length distribution were used because phase transition zones are narrow and hysteresis effects are minimized.[6b] Large quantities of such DNA are readily isolated from nucleosome cores obtained by digestion of calf thymus chromatin with micrococcal nuclease after removal of H1 histones. The most probable length is 146 ± 2 bp,[8] and greater than 90% is typically between 125 and 165 bp long. The average "hard core" axial ratio of this DNA is approximately 25, but the effective axial ratio is considerably smaller due to the counterion atmosphere.

The DNA isolation procedure utilized was partly described previously[6a,b] but will be given completely here to incorporate improvements. All procedures were conducted in the cold (4 °C) or on ice. About 100 g of frozen (−70 °C) calf thymus (Pel Freeze, Inc.) was broken into small pieces, placed in a Waring (Model 1120) blender with 500 mL of prechilled homogenization medium containing 1 mL of octanol and 1 mL of 0.1 M PMSF in 2-propanol, and then homogenized at 85 V for 5 min. (Homogenization medium was 0.25 M sucrose in 50 mM MOPS, 25 mM KCl, 5 mM $MgCl_2$, and 10 mM aminocaproic acid and was adjusted to pH 6.5 with Tris. The low pH, ϵ-aminocaproic acid, and PMSF all inhibit endogenous proteases. Nuclei remain intact in this medium.) The homogenate was filtered through 12 layers of cheesecloth (prewashed with homogenization medium) and then centrifuged at 3000 rpm for 15 min. The nuclear pellet was washed two times by resuspending in 500 mL of 0.5% Triton X-100 in homogenization medium using light blending and then centrifuging as above. This procedure was repeated two more times with homogenization medium supplemented with 2 mM $CaCl_2$. The final pellet was resuspended in 100 mL of the above solution adjusted to pH 8.0 with Tris, preincubated at 37 °C for 10 min, then incubated with 5000 units of micrococcal nuclease (Worthington), and gently shaken at 37 °C for 30 min. Digestion was terminated by adding 1 mL of 0.5 M EGTA (pH 8.0), and nuclei were recovered by centrifugation as above. Nuclei were lysed by resuspending the pellet in 200 mL of saline–EDTA (75 mM NaCl, 24 mM Na_2EDTA, adjusted to pH 6.5) and light blending in a Virtis homogenizer, and then chromatin was pelleted by centrifugation as above. The supernate chromatin was saved, and additional chromatin was solubilized by resuspending the pellet in 200 mL of 2 mM Na_2EDTA (pH 6.5) using light blending and then centrifuging at 10000 rpm for 15 min. This procedure was repeated until the chromatin concentration in the supernatant dropped below 0.5 mg/mL (determined from the absorbance at 260 nm after diluting an aliquot into 1% SDS).

Histone H1 was removed from soluble chromatin with CM-Sephadex (Pharmacia). Supernates containing chromatin were pooled and made 50 mM in NaCl by slow addition of 2 M NaCl. Dry CM-Sephadex (13 mg/mg chromatin) was added slowly, and the solution was allowed to stir for 60 min on a magnetic stirrer. Sephadex was removed by vacuum filtration and washed once with 100 mL of 50 mM NaCl in 10 mM MOPS and 0.2 mM EDTA (pH 6.8). The histone composition of the filtrate chromatin was examined by SDS gel electrophoresis[9] to verify removal of H1.

Nucleosome cores were generated by digestion of the H1-depleted chromatin with micrococcal nuclease. One-twentieth volume of 200 mM Tris, 100 mM $CaCl_2$ (pH 8.0), and micrococcal nuclease (0.5 units/50 μg of DNA) were added, and the chromatin was incubated at 37 °C for the length of time indicated by a trial digest performed on a small aliquot of sample. Digestion was terminated by addition of 1/50 volume of 0.5 M Na_2EDTA (pH 8.0). DNA products were analyzed by electrophoresis on 6% polyacrylamide gels containing SDS.[9] Proper digestion reduces >90% of the total DNA to nucleosome cores which contain few internal cleavages (DNA smaller than 140 bp).

DNA was deproteinized by Proteinase K treatment followed by phenol/chloroform extraction. Nucleosomes were precipitated by adding $MgCl_2$ to a final concentration of 10 mM and then 0.6 volumes of cold 2-propanol. After chilling in a dry ice–ethanol bath for ≥15 min, the sample was centrifuged at 8000 rpm for 15 min and the final pellet was resuspended in 0.5 M NaCl, 10 mM EDTA, 50 mM Tris–HCl, and 1% SDS (pH 8.0) to a final concentration of about 25 mg of DNA/mL. Proteinase K was added (0.5 mg/100 g of DNA), and the solution was incubated overnight at 37 °C. The solution was extracted two times with phenol–chloroform–isoamyl alcohol (24:24:1), and then DNA was precipitated with 0.8 volumes of cold 2-propanol, collected by centrifugation as above, and dried *in vacuo*. The DNA was redissolved in 50 mM NaCl in 10 mM Tris and 1 mM EDTA (pH 7.6) and digested with RNase A for 1 h at 37 °C; then RNase and any remaining protein were removed by phenol/chloroform extraction, followed by extraction twice with chloroform–isoamyl alcohol (24:1) alone. Sodium acetate was added to a final concentration of 0.3 M, and DNA was precipitated with 0.8 volumes of 2-propanol and then collected by centrifugation. The pellet was washed twice by resuspending in cold (−20 °C) 80% ethanol and then centrifuging. The final pellet was dried in vacuo.

Preparation of Samples. A large stock 1.00 M Na^+ solution was prepared consisting of 0.90 M NaCl, 50 mM sodium cacodylate, 30 mM sodium azide, and 10 mM Na_2EDTA (final pH adjusted to 6.5 with HCl). (Cacodylate and azide were used as buffers and to inhibit bacterial growth, and EDTA was used to scavenge multivalent cations and inhibit DNA degradation by trace nucleases.) All subsequent solutions were made by diluting this stock with doubly redistilled water. Solutions are referred to below in terms of the total Na^+ concentration. Glassware was routinely cleaned with nitric acid.

Purified DNA was dissolved in buffered 50 mM Na^+ and dialyzed against the same buffer for 72 h. Dialysis was performed under vacuum from a water aspirator in a collodion bag device (Schleicher and Schull) to minimize dilution. The dialysis bag was then put into dry Bio-Gel P-30 powder (Bio-Rad Labs.) to further concentration DNA. The final DNA concentration in the dialysis bag was 275 mg/mL, determined from the 258-nm absorbancy assuming an extinction coefficient of 6.6×10^3/mol DNA phosphate. Absorbance measurements were made on dilutions of 50-μL aliquots removed with a positive displacement micropipet (Drummond). The relative error of these measurements was estimated as ±2.5% on the basis of weighing of multiple aliquots removed with the micropipet.

A 400-μL aliquot of the above solution was transferred to a 2-mm path-length quartz cuvette with Teflon stopper. This aliquot and dilutions thereof were used for all NMR measurements. Subsequent DNA concentrations were prepared by diluting the original solution in the cuvette with 0.3 M Na^+ buffer. This ionic strength was chosen because the starting DNA solution had a Na^+ activity of 0.213 M, which was equal to the activity of 0.3 M Na^+ in buffer. Experiments were therefore conducted at constant sodium ion *activity*, assuming that the activity is relatively independent of DNA concentration in the range examined. We have preliminary evidence that this assumption is not valid over a wide range of DNA concentrations but is approximately valid over the range corresponding to the isotropic to cholesteric transition. Sodium ion activity was determined by using a Micro-Combination Glass Na^+ probe (Model MI-425, Microelectrodes, Inc.) connected to a Corning Model 10 pH meter.

Microscopy. DNA solutions were viewed with a Leitz Ortholux II microscope equipped with Orthomat-W camera system and white-light illumination. Polarizing filters were placed on the light stage and above the objective. Samples were contained in 2-mm rectangular cuvettes or 0.1- or 0.01-mm cylindrical, demountable cuvettes (Helma); the latter were sealed with silicon oil to prevent drying and were allowed to equilibrate at room temperature for several days before pictures were taken.

NMR Spectroscopy. Phosphorus-31 spectra were taken on nonspinning samples at a phosphorus frequency of 61.28 MHz on the "Seminole", an in-house constructed multinuclear FT spectrometer equipped with wide-bore super-conducting solenoid and quadrature detection, modified for solid-state applications. Sweep width was ±25 kHz and pulse repetition times 3 s, and 600 scans were taken for each spectrum. Gated proton decoupling was used during data acquisition.

DNA solutions contained in the 2-mm cuvette were put into a 15-mm NMR tube, and the cuvette was covered with water to prevent evaporation and condensation of solution on the cuvette walls and to facilitate heat transfer. Heating was achieved by warming a stream of air blowing through the NMR probe; temperature was controlled by a thermocouple to within ±1 °C. Each sample was examined at 10 °C intervals from 20 to 70 °C. All temperature cycles were repeated twice. For the first examination the samples were put into the magnet, kept at room temperature for 1 h, then cooled to 20 °C, and allowed to equilibrate for 30

(8) Abbreviations used are as follows: bp, base pairs; EGTA, ethyleneglycol-bis(β-aminoethyl ether)-*N,N'*-tetraacetic acid; MOPS, 3-[*N*-morpholino]propanesulfonic acid; PMSF, phenylmethylsulfonyl fluoride; SDS, sodium dodecyl sulfate.

(9) Electrophoresis of histones was performed on SDS gels according to: Thomas, J. O.; Kornberg, R. D. *Methods Cell Biol.* **1978**, *18*, 429–440. Electrophoresis of DNA was performed on 6% polyacrylamide gels according to: Maniatis, T.; Jeffrey, A.; Van de Sande, H. *Biochemistry* **1975**, *14*, 3787–3794.

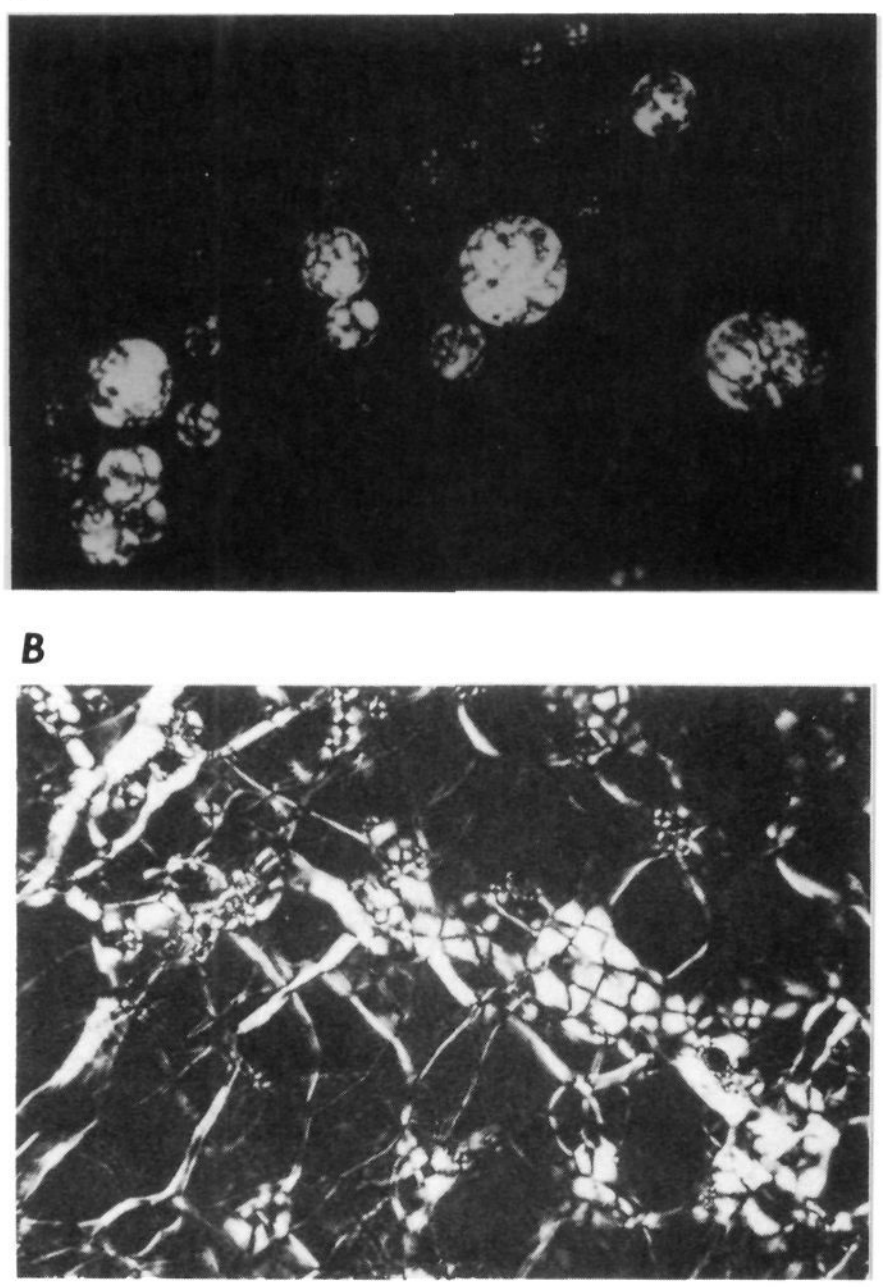

Figure 1. Liquid crystalline textures of DNA samples used for phase diagram determination. Samples were viewed through crossed polars and photographed in color but printed in black and white. The bar in B corresponds to 0.1 mm. The same magnification was used in frames A–C. (A) Cholesteric spherulites observed in 137 mg/mL sample in a cell with path length of 2 mm. (B) Fully cholesteric 220 mg/mL sample viewed in a 100-μm cuvette with planar texture and "oily streaks". (C) Magnetically ordered, fully liquid crystalline sample viewed in 2-mm cuvette. The magnetic field direction is vertical and the DNA molecules align perpendicular to the field.

min before the spectrum was taken. Data at higher temperatures were taken after equilibration for at least 30 min. After the first temperature series, the sample was removed from the magnet and left at room temperature overnight, and then the whole series was repeated. If the sample showed an isotropic resonance at a certain temperature, the cycle was repeated at 2 °C intervals to find the precise transition temperature. Thermal denaturation measurements and electrophoretic analyses on

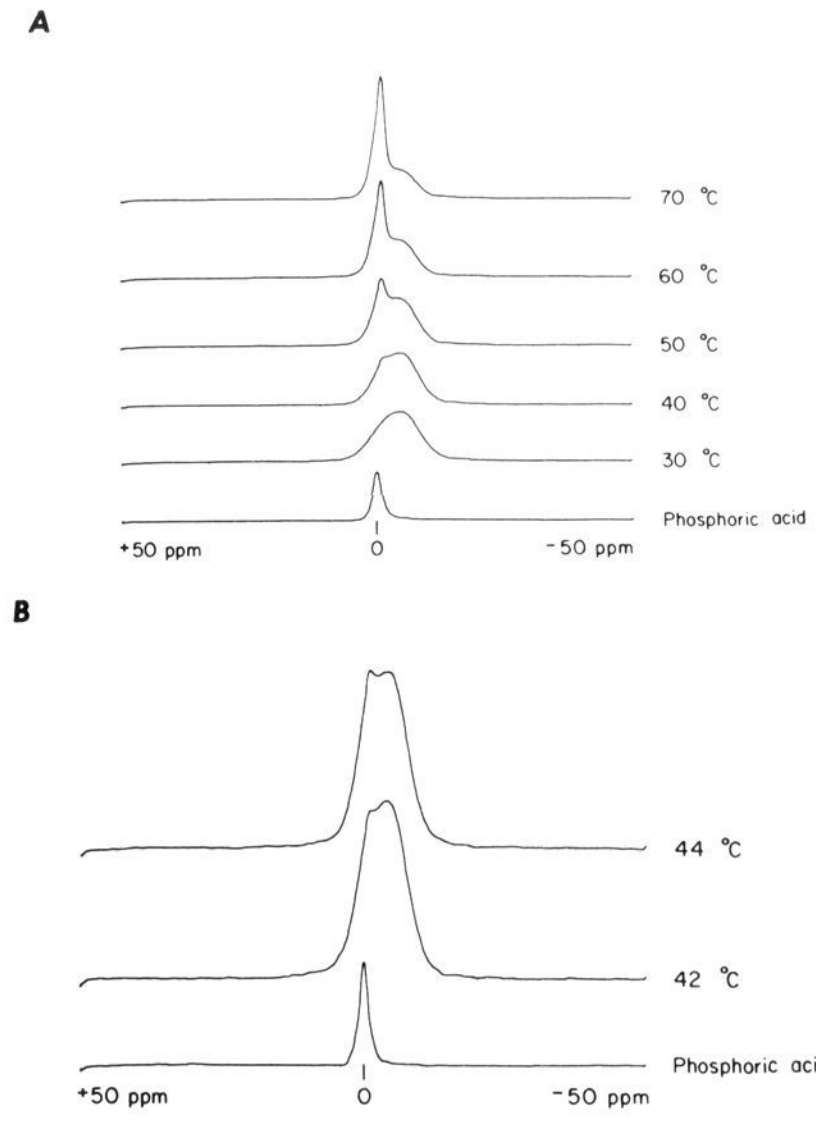

Figure 2. Temperature dependence of the solid-state phosphorus-31 resonance of the 157 mg/mL DNA sample illustrating the onset of isotropic phase formation at ca. 44 °C (frame B).

denaturing and nondenaturing gels[9] showed that DNA base pairing and chain integrity were not affected by repeated heating/cooling cycles.

Integrated resonance areas were measured from the second set of NMR data, when each sample was as fully magnetically ordered as possible, by using an Apple II+ microcomputer with graphics tablet and integration software. The accuracy of peak area determination was about 2%; hence the sample was designated as fully liquid crystalline unless the isotropic resonance was >2% of the total area.

Results

Polarizing Microscopy. Several liquid crystalline textures were observed, depending on DNA concentration. Here we present only results typical of concentrations which yielded clearly cholesteric textures and were used to determine the isotropic to cholesteric phase diagram. Samples with concentrations of 130, 137, 145, and 150 mg/mL were biphasic over the 20–70 °C range examined. The two lowest concentration samples were highly viscous and appeared transparent when viewed in the 2-mm cuvette. Microscopic examination revealed trace amounts of cholesteric phase as small spherulites. Samples with concentrations of 157 and 164 mg/mL were liquid crystalline up to 44 and 56 °C, respectively. These samples were opaque and highly iridescent and flowed easily; the properties were consistent with those of a cholesteric phase. Figure 1 shows cholesteric textures observed in some of these samples (see also ref 6b).

Solid-State ^{31}P NMR Spectroscopy and Determination of the Phase Diagram. The ^{31}P resonance observed for 157 and 164 mg/mL solutions at room temperature was reasonably symmetric and broader than expected from isotropic DNA solutions but much narrower than the powder pattern expected for a fully immobile sample. Upon heating a sharp resonance appeared on the downfield side of the broad resonance due to isotropic phase formation (Figure 2). The asymmetric disposition of the isotropic phase resonance with respect to the cholesteric phase resonance suggests that the latter phase was ordered by the magnetic field. Ordering was confirmed by polarizing microscopy (Figure 1C) and was noted in other magnetic resonance studies of similar DNA solutions.[6c] The line shape is dependent on dynamics and ordering;

Table I. The Temperature and Concentration Dependencies of the Fractions of Total DNA Molecules in the Cholesteric and Isotropic Phases[a]

concn, mg/mL	temp, °C	F_C	F_I
145	20	0.79	0.21
	30	0.81	0.19
	40	0.72	0.28
	50	0.60	0.40
	60	0.49	0.51
	70	0.29	0.71
150	20	0.92	0.08
	30	0.88	0.12
	40	0.75	0.25
	50	0.65	0.35
	60	0.48	0.52
	70	0.38	0.62
157	50	0.91	0.09
	60	0.69	0.31
	70	0.54	0.46
164	60	0.91	0.09
	70	0.85	9.15

[a] Determined from the relative integrated areas of the ^{31}P resonances of the isotropic and cholesteric phases.

hence no simple analysis of DNA dynamics in these systems was possible.

The integrated areas of isotropic and cholesteric phase resonances are proportional to the number of DNA molecules in each phase and hence can be used to establish a phase diagram. Although samples with concentrations of 130 and 137 mg/mL were biphasic, the amount of cholesteric phase was too small to detect a separate resonance, even at 20 °C. Figure 2 shows the temperature dependence of the ^{31}P spectrum for the 157 mg/mL DNA solution, which underwent a cholesteric to biphasic transition at 44 °C. Similar behavior was observed for the 164 mg/mL sample, which had a transition temperature of 56 °C. Samples of lower concentration were biphasic from 20 to 70 °C.

Isotropic to biphasic transitions of nonelectrolyte polymers in organic solvents are usually monitored by microscopic observation of spherulite formation or by increased light scattering, while the biphasic to fully liquid crystalline transition is commonly monitored by the disappearance or appearance of isotropic solvent proton NMR resonances.[3,10] Solid-state ^{31}P NMR allows direct observation of a single DNA resonance that is sensitive to mesophase formation and thereby provides an alternate, more convenient method for obtaining a quantitative phase diagram with relatively few samples.

Experimental polymer phase diagrams are normally presented in terms of the volume fraction vs. temperature. The mole fractions of total DNA molecules in isotropic and cholesteric phases were determined directly from the respective resonance areas (Table I). Calculation of volume fractions of DNA in the two phases within a biphasic solution from the mole fractions is not straightforward because the parameter of interest for a polyelectrolyte is the *effective* volume fraction, which includes the condensed counterion atmosphere.[4] The DNA *concentrations* in the fully isotropic and cholesteric phases in equilibrium at a given temperature in a biphasic solution can be determined, however, by measuring the number fractions of DNA molecules in the two phases at the same temperature for two or more samples differing in overall DNA concentration. This follows from the condition that, in the biphasic region, the composition of each phase must remain constant at constant temperature.

Briefly, let N_I = number of molecules in the isotropic phase of volume $V_I = V(1 - x)$ and N_C = number of molecules in the cholesteric phase of volume $V_C = xV$. Then C_I = DNA weight concentration in the cholesteric phase = $N_I M/(N_{Av}(1 - x)V)$, C_C = DNA concentration in the cholesteric phase = $N_C M/(N_{Av}xV)$, and $C_0 = (1 - x)C_I + XC_C$, where C_0 = the average DNA concentration, N_{Av} = Avogadro's number, and M = DNA molecular weight = (length in bp) 660. Elimination of C_I or C_C in the above

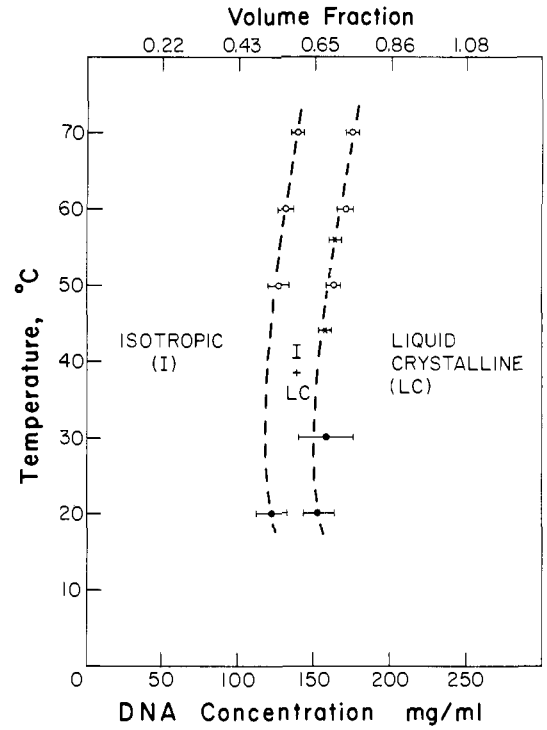

Figure 3. Phase diagram for the isotropic to cholesteric phase transitions. Points were determined by data from two samples (●), from an average of data from 3 to 4 samples (○), or directly from NMR spectra (×). Values of DNA volume fractions on the upper scale were calculated by assuming an effective DNA radius of 21 Å.

equation and substitution in terms of the mole fractions of the two phases F_I or F_C yields the pair of relationships

$$xC_C = F_C C_0 \qquad (1 - x)C_I = F_I C_0$$

At a given temperature in the biphasic region, but at different values of C_0, the above relations provide two equations in two unknowns which can be solved for C_I and C_C given measured values of F_I and F_C at the two concentrations $C_{1,0}$ and $C_{2,0}$:

$$C_C = C_{1,0}C_{2,0}(F_{C1} - F_{C2})/(C_{2,0}F_{12} - C_{1,0}F_{11})$$

$$C_I = C_{1,0}C_{2,0}(F_{11} - F_{12})/(C_{2,0}F_{C2} - C_{1,0}F_{C1})$$

The phase diagram calculated on this basis for 500-Å length DNA fragments at a sodium activity of 0.21 M is shown in Figure 3. The DNA concentration in a particular phase can be converted to the *effective* volume fraction, v, by using the relationship for the volume of a spherocylinder of length L with an assumed or calculated effective radius R:[4a] $v = CN_{Av}R^2(L + 4R/3)/M$.

Relation to Theory. The phase diagram calculated for 146 bp DNA at an Na^+ activity of 0.21 is in qualitative agreement with predictions of Flory's theory[2a] and the observed behavior[3] of rodlike nonelectrolyte polymers. That is, there is a narrow region of coexistence of the isotropic and cholesteric phases, and the phase boundaries are weakly dependent on temperature. This diagram compares well, for example, to the repulsive region of the theoretical phase diagram for rodlike molecules with an axial ratio of $x = 20$ presented by Warner and Flory,[11] who described dependencies of the concentrations at the two boundaries of the biphasic region in terms of T/T^*, where T is the actual temperature (K) and T^* is related to the free energy of anisotropic interactions between polymer segments and the average degree of disorder in the mesophase.[11,12]

The phase diagram determined for DNA is not sufficiently extensive to attempt a precise fit to the theory of Warner and Flory. It is meaningful to inquire, however, whether the two

(10) Wee, E. L.; Miller, W. G. *J. Phys. Chem.* **1971**, *75*, 1446–1452.

(11) Warner, M.; Flory, P. J. *J. Chem. Phys.* **1980**, *73*, 6327–6332.

(12) Flory, P. J.; Ronca, G. *Mol. Cryst. Liq. Cryst.* **1979**, *54*, 289–310, 311–320.

Table II. Iterative Calculation of Best-Fit Effective DNA Radii[a]

it. no.	x	y	v	v'	v/c, cm^3/g	v'/c, cm^3/g	r, Å	r', Å
				Temperature = 70 °C				
1	20	3.34	0.3806	0.5407	2.7576	3.1253	16.5	17.5
2	14.7	2.47	0.4992	0.6676	3.6172	3.858	18.8	19.4
3	13.1	2.13	0.5557	0.7275	4.0272	4.2052	19.9	20.3
4	12.4	2.02	0.583	0.7505	4.2246	4.3382	20.3	20.5
5	12.3	2.00	0.5894	0.7561	4.2707	4.3707	20.4	20.6
6	12.2	1.99	0.5919	0.7582	4.2890	4.3826	20.4	20.6
				Temperature = 20 °C				
1	20	3.34	0.379	0.541	3.081	3.558	17.4	18.6
2	13.9	2.28	0.526	0.698	4.280	4.595	20.4	21.1
3	12.0	1.96	0.598	0.764	4.866	5.026	21.8	22.1
4	11.38	1.85	0.629	0.789	5.116	5.195	22.3	22.4
5	11.18	1.81	0.639	0.798	5.197	5.248	22.4	22.5

[a] Data were fit to the theory of Flory[2a] assuming an initial axial ratio of $x = 20$. The predicted disorder parameter, y, and critical volume fractions corresponding to the isotropic/biphasic and biphasic/cholesteric boundaries, v and v', respectively, were used to estimate the effective DNA radii at these boundaries, r and r'. A new estimate of the effective axial ratio was calculated from r, and the calculation was repeated to generate new estimates of r and r' until these parameters did not change within error.

biphasic boundaries observed for DNA solutions are accurately and simultaneously predicted by the lattice statistics approach of Flory and co-workers using the effective DNA radius as the sole adjustable parameter. As a first approximation we attempted to interpret the DNA phase behavior in terms of the 1956 theory of Flory,[2a] which does not consider the anisotropy of interactions between polymer segments and treats the equilibrium degree of disorder in a simpler manner than that adopted by Warner and Flory. This simplification is justified in part by the observations that the phase boundaries predicted for athermal polymer solutions by the two theories are very similar, and the isotropic and cholesteric boundaries for DNA solutions were weakly temperature dependent, suggesting that the anisotropy of interactions between DNA segments is weak to a first approximation.

A simple iterative procedure was used to determine the best-fit effective DNA radius, and hence axial ratio, which reproduced the DNA concentration at the isotropic/biphasic and biphasic/cholesteric boundaries at 20 and 70 °C. Briefly, the volume fractions corresponding to the above phase boundaries were initially calculated assuming an effective axial ratio of 20. The effective DNA radii corresponding to these volume fractions were calculated from the known DNA concentrations as described previously. A revised estimate of the effective axial ratio was then calculated from the radius determined from the isotropic/biphasic boundary and used to provide new estimates of the effective radii at the two phase boundaries. This procedure was repeated until revised estimates of the axial ratio yielded no significant changes in the estimated radii. At this point radii calculated from the two phase boundaries also converged to values that were identical within error (Table II). Values calculated for the two boundaries were 22.3 and 22.4 Å, respectively, at 20 °C and 20.4 and 20.6 Å, respectively, at 70 °C. (The latter values were not corrected for water expansion.) These radii are in excellent agreement with the effective DNA radius of 21 Å, in solutions with a supporting electrolyte concentration of 0.2 M NaCl, determined from analyses of the sedimentation equilibrium distribution of concentrated DNA solutions by using scaled particle theory by Brian et al.,[4a] and with theoretical calculations.[4b-d] Evidently the effective DNA radius is relatively insensitive to temperature. This is due in part to the fact that the decrease in effective axial ratio with increasing radius is offset by the accompanying increase in effective particle volume. The effective axial ratio required for phase separation of these DNA fragments is approximately 12 (Table II), only modestly above the predicted minimum required for phase separation.[2a,12]

Higher Order Phase Transitions. Examination of solutions more concentrated than those required to reach the biphasic/cholesteric boundary provided additional verification of the above estimate of the effective DNA radius. The effective volume fractions calculated at the isotropic/biphasic and biphasic/cholesteric boundaries at 20 °C were 0.63 and 0.79, respectively; hence there is little "free volume" in the biphasic or fully cholesteric DNA solutions. Extrapolation of the concentration dependence of the volume fraction assuming an effective radius of 21.4 Å predicts an effective volume fraction exceeding 1.0 at concentrations above 220 mg/mL. The fact that we have prepared solutions up to 275 mg/mL in the same buffer suggests that reordering of the DNA rods, counterion atmosphere, solvent, or combination of the above must occur to create the required free volume.

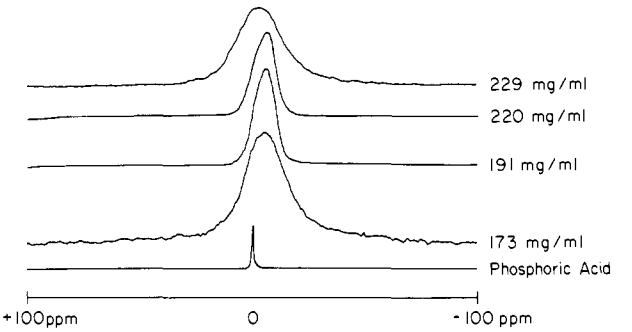

Figure 4. Concentration dependence of the solid-state phosphorus-31 NMR line width. Microscopic textures of 191 and 220 mg/mL samples were consistent with a fully cholesteric phase and were different from that of the 229 mg/mL sample. Spectra were obtained at 20 °C.

Evidence for DNA reordering was provided by solid-state ^{31}P NMR spectra of more concentrated DNA samples. The cholesteric phase resonance line width progressively broadened as the biphasic region was traversed in the direction of increasing DNA concentration and then abruptly dropped at concentrations above the biphasic/cholesteric boundary (Figure 4). The line shape also changed at this point from approximately Gaussian to an asymmetric shape typically expected from rotational averaging. We attribute the latter changes in resonance line width and shape to magnetic ordering of the cholesteric phase and subsequent reduction in chemical shift anisotropy.[6b,c] Magnetic ordering is resisted in biphasic solutions because the cholesteric phase is confined to spherulites by surface tension forces.

The ^{31}P resonance line width and shape remained relatively constant from 173 to 220 mg/mL but then abruptly broadened and became near Gaussian at concentrations of 229 and 239 mg/mL. By analogy to the behavior of biphasic (isotropic/cholesteric) solutions, we suggest that this line width broadening is due to partial formation of a more condensed phase. Resonance narrowing is expected to be optimal when the solution is monophasic, since molecules at the interfaces of biphasic domains will tend to be disordered on the average. Preliminary examinations with the polarizing microscope showed that these samples had textures different from those of the cholesteric phase.

Discussion

Short DNA fragments behave in solution like near rigid, rodlike particles. Solutions of such particles should separate into isotropic and anisotropic phases above a critical polymer concentration that

varies approximately inversely with axial ratio (for modest axial ratios).[1-3] Although theories of the behavior of nonelectrolyte rods do not strictly apply to solutions of charged particles, DNA molecules in aqueous solution can be treated in some contexts as "scaled" spherocylindrical rods with an effective radius dependent on the distance from the DNA surface required for the electrostatic repulsion potential to drop to $kT/2$.[4a]

We were able to fit the DNA concentrations at the observed isotropic/biphasic and biphasic/cholesteric phase boundaries at 20 or 70 °C to volume fractions predicted by Flory's theory with a single effective radius. The best-fit radii obtained at the two temperatures agreed well with the effective radii obtained for more dilute DNA solutions at a similar Na^+ concentration by sedimentation equilibrium[4a] and with the effective radius calculated from Poisson-Boltzmann statistics.[4b,d] Since electrostatic repulsion is the greatest obstacle to close packing of DNA molecules in solution, one expects that increasing ionic strength will cause a decrease in effective DNA radius and an increase in the critical DNA concentration necessary for liquid crystalline phase formation. Observations of Brian et al.[4a] were consistent with this prediction. A preliminary phase diagram for isotropic to cholesteric transitions in DNA solutions of high ionic strength (ca. 2 M) was described by Rill.[6b] The biphasic region at this sodium concentration was shifter toward higher DNA concentrations by about 60 mg/mL in comparison to the phase diagram presented in this paper. Previous studies also demonstrated an approximate inverse relationship between DNA length and the critical concentration at the isotropic/biphasic boundary.[6a] Together these results show that the isotropic to cholesteric phase transitions of DNA can be treated, to a first approximation, in terms of scaled particles within the context of the lattice statistics formalism of Flory and co-workers.[2a,b]

The unusual dependence of the ^{31}P line width on DNA concentration at concentrations above the fully cholesteric range can be interpreted most simply in terms of formation of a more highly ordered phase. This transition occurred abruptly over a narrow range of DNA concentrations, suggesting that major changes in DNA organization can occur readily despite the high macroscopic viscosities of these solutions. DNA concentrations occurring in vivo commonly approach or exceed those examined here, and the critical concentrations required for rodlike polymer phase transitions decrease with increasing length. As pointed out by Flory,[2a] the behavior of long, semiflexible polymers is expected to be intrinsically similar to that of shorter, rodlike analogues. The ready ability of rodlike DNA molecules to assume alternate liquid crystalline forms may, therefore, be of significance to mechanisms of DNA packing in vivo.

Acknowledgment. We are grateful to Dr. Penny Gilmer for use of her Leitz microscope and to Drs. Timothy Cross, Robert Fulton, and Theodore Williams for reading the manuscript and discussion.

Wavelength-Dependent Primary Photoprocesses of $Os_3(CO)_{12}$ in Fluid Solution and in Rigid Alkane Glasses at Low Temperature: Spectroscopic Detection, Characterization, and Reactivity of Coordinatively Unsaturated $Os_3(CO)_{11}$

James G. Bentsen and Mark S. Wrighton*

Contribution from the Department of Chemistry, Massachusetts Institute of Technology, Cambridge, Massachusetts 02139. *Received July 8, 1986*

Abstract: Wavelength-dependent photochemistry is reported for $Os_3(CO)_{12}$ in hydrocarbon solutions at 298 and 195 K and in rigid hydrocarbon glasses at 90 K. Near-UV and vis irradiation of 0.2 mM $Os_3(CO)_{12}$ at 298 K in alkane solutions containing 5 mM L yields mainly $Os_3(CO)_{11}L$ (L = PPh_3, $P(OMe)_3$) as the initial photoproduct with a wavelength-dependent quantum yield: $\Phi_{436nm} < 0.0001$, $\Phi_{366nm} = 0.017 \pm 0.001$, and $\Phi_{313nm} = 0.050 \pm 0.003$ for L = PPh_3, independent of the presence of added 0.1 M tetrahydrofuran. Photosubstitution of PPh_3 for CO is not affected by added 1 M CCl_4, and the 366 nm quantum yield does not change on increasing the PPh_3 concentration to 0.10 M, consistent with photodissociative loss of CO from an upper level excited state. Electronic spectral features for $Os_3(CO)_{12}$ become well-resolved in an alkane glass of 90 K; low-energy excitation into the first (382 nm: $10a_1' \rightarrow 16e'$; $^1A_1' \rightarrow {}^1E'$) or second (320 nm: $15e' \rightarrow 6a_2'$; $^1A_1' \rightarrow {}^1E'$) absorptions for $Os(CO)_{12}$ yields no net photochemistry in the 90 K alkane glass. However, excitation into the third electronic absorption (278 sh nm: $14e' \rightarrow 6a_2'$; $^1A_1' \rightarrow {}^1E'$) of 0.1 mM $Os_3(CO)_{12}$ yields loss of one CO as the only FTIR detected photoreaction to yield a single product, formulated as axially vacant $Os_3(CO)_{11}$ on the basis of FTIR and UV-vis spectral characterization and reaction chemistry. While the photogenerated $Os_3(CO)_{11}$ reacts with ^{13}CO at low temperature to give the axial-^{13}CO-$Os_3(CO)_{11}(^{13}CO)$, UV irradiation of axial-^{13}CO-$Os_3(CO)_{11}(^{13}CO)$ in a 90 K methylcyclohexane glass yields dissociative CO loss in a ratio of $^{12}CO/^{13}CO$ of greater than 28. These results suggest photodissociative loss of equatorial CO from $Os_3(CO)_{12}$, followed by rearrangement of equatorially vacant $Os_3(CO)_{11}$ to the axially vacant form. Photogenerated $Os_3(CO)_{11}$ reacts with two electron donor ligands to yield $Os_3(CO)_{11}L$ complexes (L = N_2, C_2H_4, PPh_3, 1-pentene, 2-MeTHF) and with H_2 to yield $H_2Os_3(CO)_{11}$. The $H_2Os_3(CO)_{11}$ complex has been detected by FTIR as an intermediate in the direct photoconversion ($\Phi_{366nm} = 0.02$) of $Os_3(CO)_{12}$ to $H_2Os_3(CO)_{10}$ in H_2-saturated alkane solutions at 298 K. Near-UV irradiation of $H_2Os_3(CO)_{11}$ cleanly yields $H_2Os_3(CO)_{10}$ and free CO at 298 or 90 K. Selective excitation into the second absorption of $Os_3(CO)_{12}$ at 90 K yields inefficient associative photosubstitution of strong π-acceptors (C_2H_4, C_5H_{10}, ^{13}CO) but not N_2 or 2-MeTHF for CO. In fluid solutions, competitive photofragmentation is correlated with long wavelength irradiation and with strong π-acceptor ligands (CO, C_2H_4, not PPh_3).

We report here a detailed characterization of the electronic, structural, and chemical properties of photogenerated, coordinatively unsaturated $Os_3(CO)_{11}$. The $Os_3(CO)_{11}$ can be photogenerated in rigid alkane glasses at low temperature according to eq 1. This article includes a detailed investigation of the wavelength dependent competition between dissociative CO loss

0002-7863/87/1509-4518$01.50/0